ACS APPLIED MATERIALS & INTERFACES

Research Article

www.acsami.org

Vapor Coating Method Using Small-Molecule Organic Surface Modifiers to Replace N-Type Metal Oxide Layers in Inverted Polymer Solar Cells

Hyosung Choi, Hak-Beom Kim, Seo-Jin Ko, Gi-Hwan Kim, and Jin Young Kim*

School of Energy and Chemical Engineering, Ulsan National Institute of Science and Technology (UNIST), Ulsan, 689-798, South Korea

Supporting Information

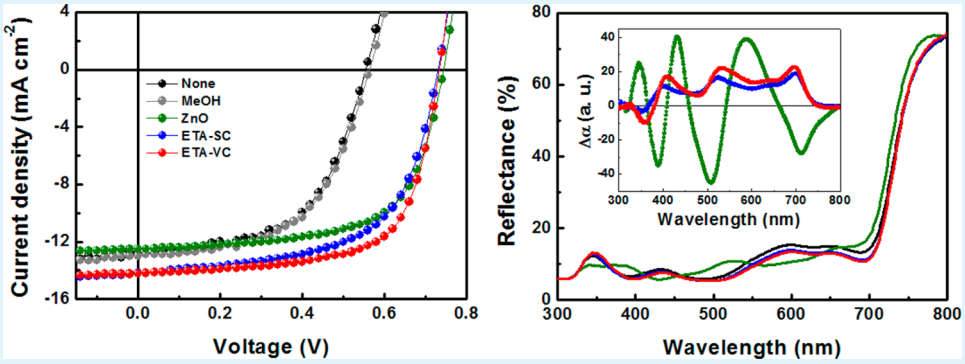

ABSTRACT: We investigate a simple fabrication method for vapor coating small-molecule organic interlayers as replacements for metal oxide films. The interfacial layers, which serve both as both surface modifiers to reduce the substrate work function and electron selective layers, maximize light absorption within the active layer while improving electron transport and compatibility between the active layer and cathode, leading to a ~22% enhancement in power conversion efficiency and similar air stability compared to devices using a ZnO layer.

KEYWORDS: *organic surface modifier, vapor coating, metal oxides, electron selective layer, inverted polymer solar cells*

INTRODUCTION

Polymer−fullerene bulk heterojunction (BHJ) polymer solar cells (PSCs) have been regarded as next-generation solar cells because of their advantages such as low-cost, lightweight, and flexible device fabrication.[1−4] Substantial efforts synthesizing new semiconducting polymers and metal nanoparticles, developing device architectures, and controlling the active layer morphology have improved the power conversion efficiencies (PCE) of conventional PSCs (cPSCs) up to 9%.[5−10] In spite of dramatic improvements in device efficiency, there remains a major concern about the stability of cPSC devicess for commercialization.[11] Poor stability of cPSCs largely originates from the acidic nature of poly(3,4-ethylenedioxythiophene):polystyrene sulfonic acid (PEDOT:PSS) and easily oxidized low work function metal cathodes (e.g., calcium, aluminum).[12,13] In order to resolve these issues, inverted PSCs (iPSCs) have been developed, where high work function metals (e.g., gold, silver) and metal oxides (e.g., titanium dioxide, zinc oxide, molybdenum oxide) are used as anode and electron/hole transport layers, respectively.[4,14−17] Metal oxides have been widely used for iPSCs because of their high charge-carrier mobilities and transparency in the visible spectrum.[18,19] However, there are drawbacks to the use of metal oxides including inherent incompatibility between inorganic metal oxides and organic active layers, high processing temperatures required to prepare oxide films, light absorption in the UV region and optical interference effects, all which may degrade device performance.[12,20−22] To overcome these problems, polymer surface modifiers, such as polyethylenimine ethoxylated (PEIE) and poly[(9,9-bis(3′-(*N*,*N*-dimethylamino)-propyl)-2,7-fluorene)-*alt*-2,7-(9,9-dioctylfluorene)] (PFN), have been employed to decrease cathode work functions without relying on oxide layers in iPSCs.[4,23,24] In particular, PEIE layers deposited on top of various layers (metal oxides, metal, conducting polymer, and graphene, etc.) via spin-coating can effectively reduced their work functions while providing excellent electron selectivity, leading to performance comparable to devices using metal oxide layers.[23] However, polymer surface modifiers require synthesis/purification processes and should be dissolved in polar solvents (e.g., 2-methoxyethanol, methanol, isopropanol, etc.) for spin-coating. In addition, the thickness should be adjusted for device optimization by controlling the solution concentration and spin-coating rate. In spite of a need to develop new surface modifiers and coating

Received: January 6, 2014
Accepted: April 10, 2014
Published: April 10, 2014

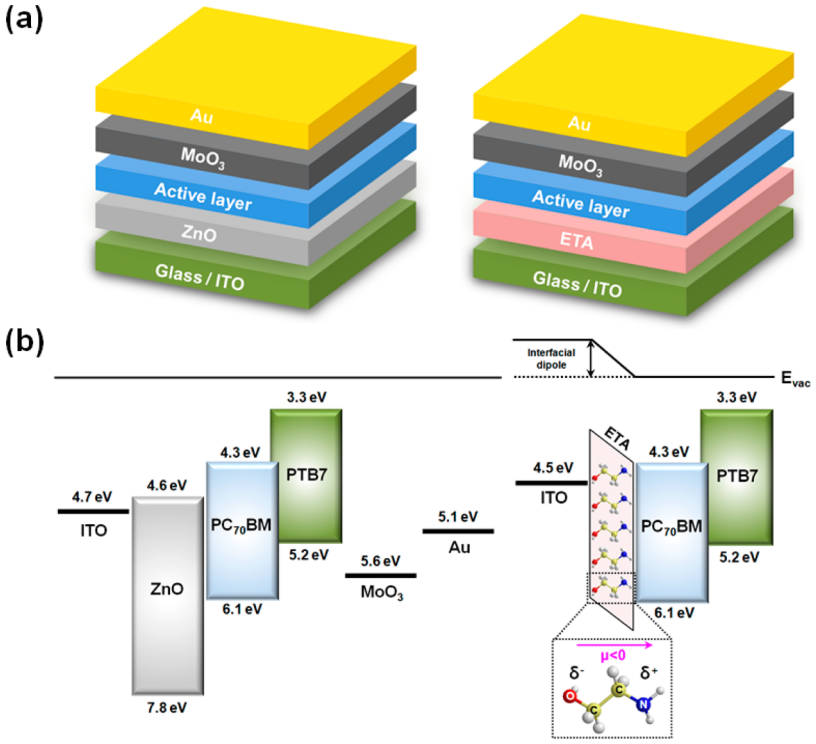

Figure 1. (a) Device architecture and (b) energy band diagram of iPSCs incorporating a ZnO layer or ETA treatment.

methods, there have been no reports on small-molecule organic surface modifiers or new coating techniques for high performance iPSCs (Supporting Information Table S1).

In this work, we introduce a vapor coating method using small-molecule, organic, surface modifiers to fabricate high performance iPSCs. Ethanolamine (ETA) is used as both a surface modifier and electron selective layer in iPSC devices. Since ETA is soluble in polar solvents and has an appreciable vapor pressure, ETA can be easily deposited on ITO substrates via both spin- (ETA-SC) and vapor-coating (ETA-VC). ETA treatment reduces the work function of indium tin oxide (ITO) cathode, facilitating electron transport while blocking hole transport from the active layer to cathode. Furthermore, ETA treatment maximizes light absorption within the active layer due to the absence of light absorption in the visible or UV regions, and does not lead to unwanted reflection or interference effects that accompany the use of metal oxide layers, leading to enhancement in short-circuit current density (J_{SC}) and PCE.

EXPERIMENTAL SECTION

PSCs Fabrication and Characterization. ITO-coated glass substrates were cleaned by sequential ultrasonication in deionized water, acetone, and iso-propanol, followed by drying in an oven overnight. The ZnO precursor solution was prepared via sol–gel method.[25] For ZnO layers (50 nm), the precursor solution was spin-cast on ITO substrates at 3000 rpm for 25 s and then annealed at 110 °C for 10 min. For ETA-SC, ETA was dissolved in methanol (MeOH) (optimized concentration of 2 wt %) and this solution was spin-cast onto ITO substrates at 2000 rpm for 40 s. To remove physically adsorbed ETA molecules, ETA-SC-treated films were washed with pure MeOH by spin-coating MeOH on them, leading to the formation of an ETA monolayer. For ETA-VC, a few ETA droplets (40 μL) were dropped around ITO substrates inside a Petri dish and the Petri dish was closed. Subsequently, the temperature was increased to 50 °C and maintained for 10 min. For deposition of the active layer, blend solutions of PTB7 (1 wt %)/$PC_{70}BM$ (1.5 wt %) dissolved in a mixed solvent of consisting of chlorobenzene and 1,8-diiodooctane were spin-coated on top of the treated substrates in a nitrogen-filled glovebox. The thickness of the active layer was measured to be about 190 nm. Device were then brought under vacuum (<10^{-6} Torr), and p-type MoO_3 (5 nm) and Au (80 nm) electrodes were then deposited via thermal evaporation. The area of the Au electrode defines the active area of the device as 13.0 mm^2. For the characterization of PSCs, current density–voltage (J–V) characteristics were measured using a Keithley 2635A Source Measure Unit. Solar cell performance was measured under Air Mass 1.5 Global (AM 1.5 G) simulated solar irradiation with an intensity of 100 $mW{\cdot}cm^{-2}$. EQE measurements were obtained using a PV measurement QE system using monochromated light from a xenon arc lamp under ambient conditions. The monochromatic light intensity was calibrated using a Si photodiode and chopped at 100 Hz. A mask (13.0 mm^2) made of thin metal was used for J–V characteristics and EQE measurements.

Characterization of ITO Electrodes with ZnO or ETA Treatment. The work function of ITO electrodes with ZnO layers and ETA treatment were obtained via ultraviolet photoelectron spectroscopy using He I (21.22 eV) radiation line from a discharge lamp. AFM images (1.5 μm × 1.5 μm) were obtained using a VeecoAFM microscope in a tapping mode. Reflectance spectra were measured on a Varian Cary 5000 spectrophotometer. Contact angles were measured using DSA100 (KRUSS, Germany). Impedance spectra were measured using an impedance analyzer (SI 1287 Solartron). The oscillation amplitude of the AC voltage was maintained at 10 mV for all impedance measurements. ZnO layer thickness was measured using a Surface Profiler (KLA Tencor).

RESULTS AND DISCUSSION

Figure 1a and 1b shows device structures and energy-band diagram of iPSCs incorporating ZnO layers or ETA treatment, respectively. The ZnO nanoparticles were prepared via a sol–gel method.[25] The ZnO layer was introduced between ITO and the active layer and served as an electron selective layer (Figure 1a) because of the large band gap (3.2 eV) and well-matched energy levels with the components of the active layer. The

dx.doi.org/10.1021/am500092a | ACS Appl. Mater. Interfaces 2014, 6, 6504–6509

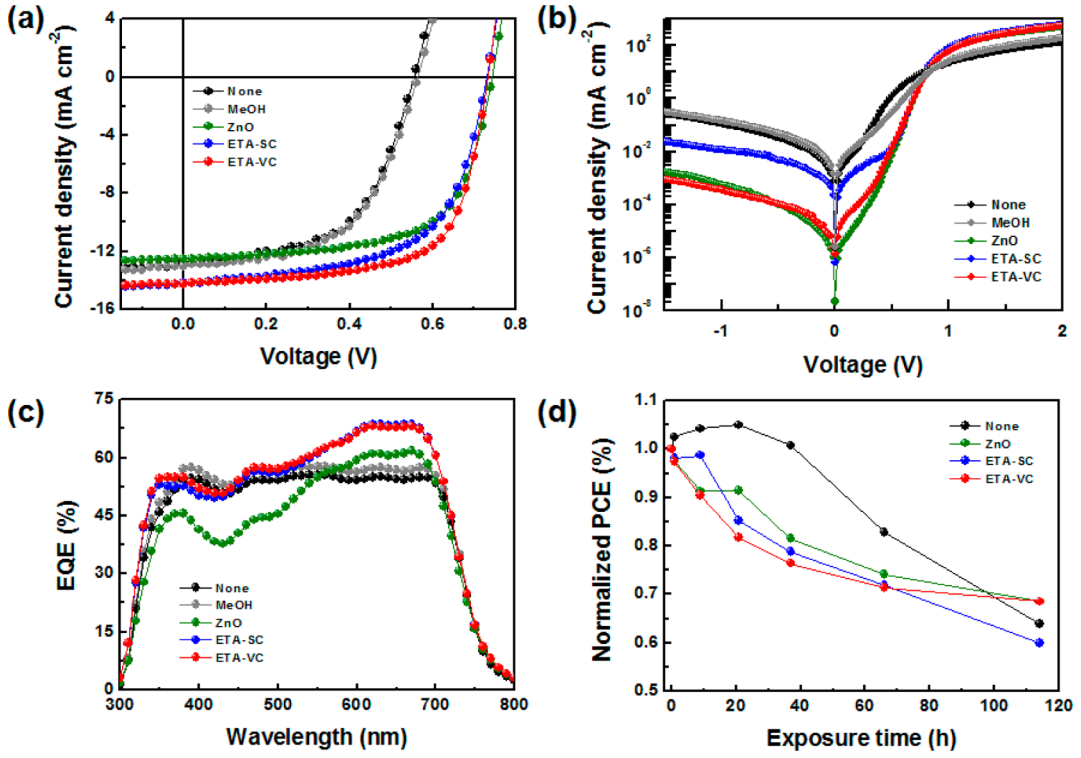

Figure 2. $J-V$ characteristics under (a) A.M. 1.5G illumination and (b) dark condition, (c) EQE, and (d) air stability of PTB7:$PC_{70}BM$-based iPSCs with different treatments.

Table 1. Device Characteristics of PTB7:$PC_{70}BM$-Based iPSCs with Different Treatments

device configuration	J_{SC} (mA cm^{-2})	V_{OC} (V)	FF	PCE (%)	J_{SC} [calcd] (mA cm^{-2})	$R_s{}^a$ (Ω cm^2)	$R_{sh}{}^a$ (Ω cm^2)
ITO/PTB7:$PC_{71}BM$	12.90	0.56	0.56	4.02	12.50	1.53	270
ITO/MeOH/PTB7:$PC_{70}BM$	13.00	0.56	0.56	4.13	13.01	1.48	350
ITO/ZnO/PTB7:$PC_{70}BM$	12.50	0.74	0.65	6.00	12.11	1.10	791
ITO/ETA-SC/PTB7:$PC_{70}BM$	14.20	0.73	0.61	6.28	14.01	1.19	469
ITO/ETA-VC/PTB7:$PC_{70}BM$	14.23	0.73	0.67	6.99	14.08	1.02	1268

$^a R_s$ and R_{sh} were derived from the slope of $J-V$ curves at open-circuit ($I = 0$) and short-circuit ($V = 0$) condition, respectively.

valence band energy of 7.8 eV and conduction band energy of 4.6 eV serve to block hole extraction and facilitate electron transport from the active layer to the cathode. For ETA-SC, ETA was dissolved in methanol (MeOH) and this solution was spin-coated on top of ITO substrates. The vapor-coating method is similar to solvent annealing of PSCs. After putting several ITO substrates in glass dish, 3−5 drops (40 μL) of ETA were placed in the vicinity of substrates and the Petri dish was covered. Subsequently, the temperature was increased to 50 °C and maintained for 10 min. The details of ETA-SC and ETA-VC are described in the Experimental Section. As shown in Figure 1b, an interfacial dipole is formed by ETA-SC and ETA-VC layers, shifting the vacuum level of ITO close to that of the active layer and effectively reducing work function of bare ITO (4.74 eV) to 4.52 and 4.48 eV, respectively (Supporting Information Figure S1 and Table S2). This implies that ETA treatment can be used without a metal oxide layer to facilitate electron transport from the active layer to the cathode by reducing the energy barrier between them.

To compare the effect of ZnO and ETA on device performance both as a surface modifier and electron selective layer, iPSCs were fabricated using poly[[4,8-bis[(2-ethylhexyl)-oxy]benzo[1,2-b:4,5-b′]dithiophene-2,6-diyl][3-fluoro-2-[(2-ethylhexyl)carbonyl]-thieno-[3,4-*b*]thiophenediyl]] (PTB7) and [6,6]-phenyl-C_{70} butyric acid methyl ester ($PC_{70}BM$) as the active layer (Figure 1a). Figure 2a and 2b exhibit current density−voltage ($J-V$) characteristics of PTB7:$PC_{70}BM$ iPSCs with different electron selective layer under AM 1.5 irradiation and dark condition, respectively. The device without any treatment was used as a reference. We also prepared devices with MeOH treatment to understand if MeOH alone had any effect on device performance; MeOH treatment alone did not significantly affect device characteristics. The device with the ZnO layer exhibited a J_{SC} of 12.5 mA cm^{-1}, open-circuit voltage (V_{OC}) of 0.74 V, fill factor (FF) of 0.65, and PCE of 6.00%. Both ETA-SC and ETA-VC treatments instead of ZnO layer remarkably improved J_{SC} up to 14.20 mA cm^{-1}, whereas V_{OC} and FF remained similar (V_{OC} = 0.73 V, FF = 0.61 for ETA-SC and V_{OC} = 0.73 V, FF = 0.67 for ETA-VC). Detailed device characteristics are listed in Table 1. Compared to the device with ZnO, the device with ETA-SC showed a decrease in *FF*, whereas a slightly increased FF is observed in the device with ETA-VC. Slight changes in *FF* by different treatments are consistent with differences in the leakage currents and rectification ratios of dark $J-V$ characteristics (Figure 2b). These tendencies were also supported by the observed series (R_s) and shunt resistances (R_{sh}) (Table 1). The PCE enhancement by both ETA-SC and ETA-VC treatments mainly

dx.doi.org/10.1021/am500092a | *ACS Appl. Mater. Interfaces* 2014, 6, 6504−6509

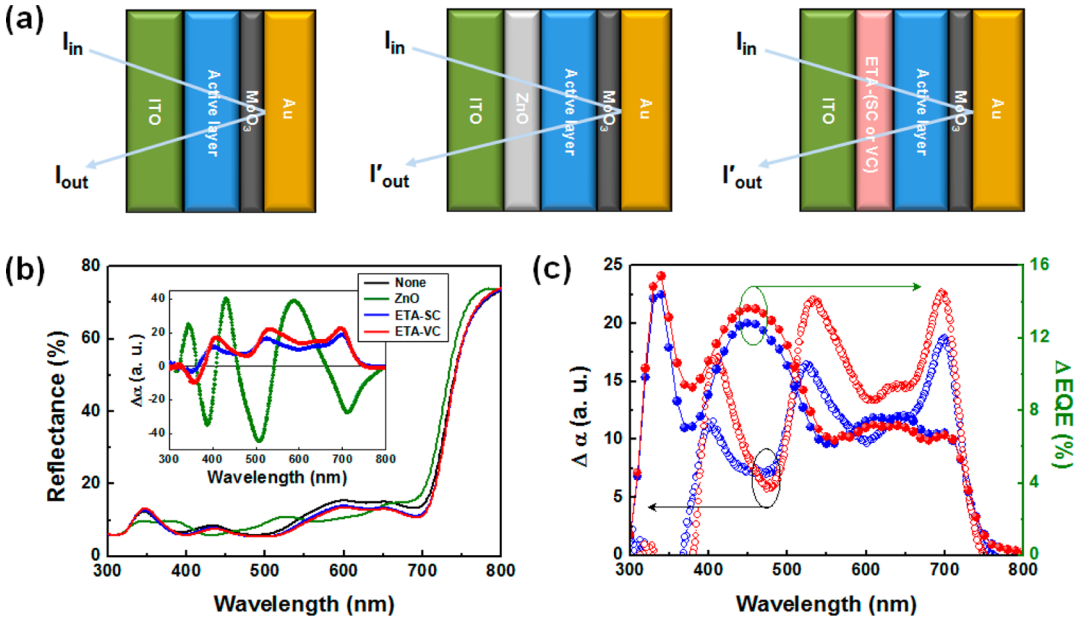

Figure 3. (a) Device structures for reflectance measurement and (b) reflectance spectra of PTB7:$PC_{70}BM$-based iPSCs with different treatments. (c) Comparison of absorption change ($\Delta\alpha$) with EQE enhancement (Δ EQE) by ETA-SC and ETA-VC treatments. The inset of panel b shows $\Delta\alpha$ within the whole device architecute by ZnO layer or ETA treatment.

resulted from a ~14% increase in J_{SC}, which can clearly be seen in the EQE results (Figure 2c). Although the device with ZnO produced a J_{SC} similar to that of the reference device, we observed changes in the shape of the EQE curves. The EQE values of the device with ZnO were lower in the short wavelength region (below 560 nm) and higher in longer wavelength region (above 560 nm), compared to reference device. In contrast, both ETA-SC and ETA-VC treatment led to remarkable EQE enhancement over the entire visible spectrum. The different shape of the EQE of the device with ZnO may be attributed to the combined effects of light absorption in UV region and reflection/interference effects caused by ZnO layer. Since device stability in air condition is one of key motivations to study iPSCs, we also tested air stability of iPSCs with different electron selective layers for over 120 h (Figure 2d). After air exposure of the devices with different electron selective layers for 120 h, device efficiencies were reduced by 32% for ZnO, 40% for ETA-SC, and 32% for ETA-VC, respectively. In spite of the absence of a metal oxide layer, air stability of the devices with ETA-VC was comparable to that of the ZnO device. Furthermore, ETA treatments are suitable for flexible devices and roll-to-roll mass production because of their solution processability at low temperature.

To understand the effect of ETA treatment on device performance, we investigated changes in light absorption from reflectance measurements of devices with different electron selective layers and otherwise identical architectures (Figure 3a). Figure 3b shows reflectance spectra of the devices with different electron selective layers. The shapes of reflectance spectra are similar in all devices except for the ZnO device. To understand the changes in light absorption within the active layer caused by ZnO and ETA, we calculated the absorption change ($\Delta\alpha$) from the results of reflectance measurements (inset of Figure 3b).[9,26] Compared to the reference device, the device with the ZnO layer showed a significant decrease in light absorption due to interference, whereas both ETA treatments led to enhanced light absorption in the range of 400−750 nm. To determine the origin of J_{SC} enhancement, we also compared the $\Delta\alpha$ and EQE enhancement (Δ EQE) for devices with different ETA treatments. For calculation of Δ EQE, we subtracted EQE of the devices with the ZnO layer from EQE of the devices with ETA treatments (Figure 3c). The Δ EQE spectra of ETA-SC and ETA-VC showed high and broad enhancement over the whole visible spectrum, consistent with changes in absorption ($\Delta\alpha$). This implies that increases in J_{SC} upon replacing ZnO with ETA originate from remarkable increases in light absorption within the active layer.

To investigate changes in hydrophobicity and morphology of the ITO surface with different treatments, we measured contact angles and atomic force microscopy (AFM) of ZnO-coated and ETA-treated ITO substrates (Supporting Information Figure S2). We used bare ITO as a reference. ITO without UV ozone treatment showed a contact angle of 79° (Supporting Information Figure S2a) and surface roughness of 0.80 nm (Supporting Information Figure S2e). After depositing a ZnO layer on the ITO substrate, the contact angle decreased to 33° (Supporting Information Figure S2b) while surface roughness increased to 1.52 nm (Supporting Information Figure S2f). Compared to the ZnO layer, both films with ETA-SC and ETA-VC treatment showed increased contact angles (SC: 44° and VC: 64°) (Supporting Information Figure S2c and S2d) and lower root-mean-square roughness (RMS) surface roughness (SC = 0.48 nm and VC = 0.55 nm) (Supporting Information Figure S2g and S2f). To optimize processing conditions for ETA-VC deposition, we fabricated devices and measured contact angles as a function of vapor exposure time. Increasing the exposure time reduced J_{SC} and FF, which implies that excessive ETA vapor interaction with the ITO substrate is detrimental for device performance (Supporting Information Figure S4 and Table S3). In contact angle measurements, there were negligible changes in contact angles with increasing vapor time (Δ contact angle between ETA-VC for 10 and 90 min = 4°) (Supporting Information Figure S5). These results indicate an optimal ETA vapor exposure time of 10 min, which is

dx.doi.org/10.1021/am500092a | ACS Appl. Mater. Interfaces 2014, 6, 6504−6509

sufficient to deposit ETA molecules on the ITO substrate and leads to optimal device performance. Although ETA treatment increases the hydrophobicity of the ITO surface and makes the surface of the electrode smoother, the adsorbed ETA layer has no influence on the morphologies and thickness of the PTB7:$PC_{70}BM$ active layer (Supporting Information Table S4). The RMS roughness (1.50 ± 0.05 nm) and thicknesses (190 ± 25 nm) of active layers on ITO substrates were almost identical regardless of ZnO or ETA treatments.

To elucidate the influence of ETA treatment on recombination losses and charge transport between the organic active layer and metal oxide layer, we measured the dependence of V_{OC} on the logarithm of the light intensity using electrical impedance spectroscopy (EIS). The light intensity dependence of V_{OC} provides the order of the recombination processes in BHJ PSCs.[27−29] A linear dependence of V_{OC} on the logarithm of light intensity, with a slope of kT q^{-1} has been commonly observed in BHJ PSCs because of bimolecular recombination

$$\delta V_{OC} = \left(\frac{kT}{q}\right)\ln(I) + \text{constant} \quad (1)$$

where k is Boltzmann's constant, T is the temperature in Kelvin, and q is the elementary charge.[27,30] As shown in Figure 4a, the ETA-SC device showed a stronger dependence of V_{OC} on the logarithm of light intensity, with slope of 1.20 $kT\ q^{-1}$ compared to a slope of (1.09 $kT\ q^{-1}$) for the ZnO device. In contrast, the device with ETA-VC exhibited a reduced dependence of V_{OC} on logarithm of light intensity with slope nearly equal to 1.0 $kT\ q^{-1}$. Since a strong dependence of V_{OC} on light intensity indicates high trap-assisted recombination, these results show that ETA-VC treatment remarkably reduced recombination rates at the interface of the active layer and ITO cathode, compared to ZnO and ETA-SC. EIS results are also consistent with these data (Figure 4b); the ETA-SC device showed higher charge transfer resistance (R_{CT}) than ZnO device, whereas ETA-VC treatment remarkably reduced R_{CT}. We can speculate that well-aligned ETA molecules on the ITO surface by slow vapor coating facilitate electron transport from the active layer to the cathode. The decreases in trap-assisted recombination and R_{CT} by ETA-VC treatment improves charge collection probability and electron transport from the active layer to cathode, leading to high J_{SC} and FF.

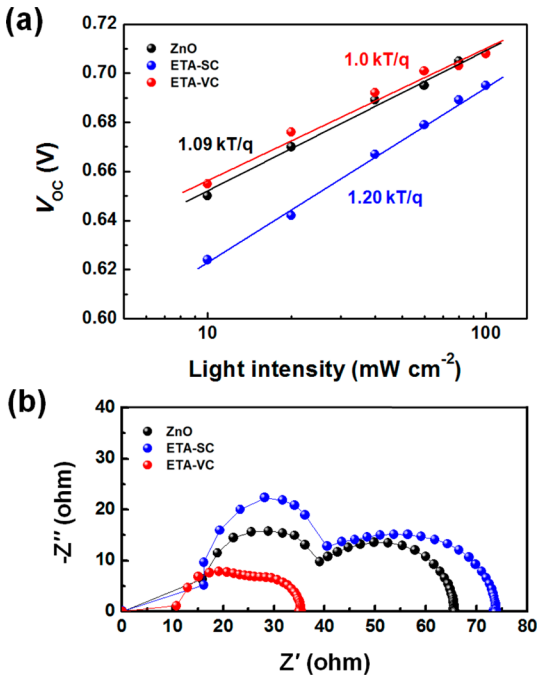

Figure 4. (a) Dependence of V_{OC} on light intensity and (b) electrical impedance measurement of PTB7:$PC_{70}BM$ iPSCs with different treatments.

CONCLUSIONS

In conclusion, a vapor coating method to deposit an interfacial ETA layer between the active layer and ITO electrode has been developed used to prepare high performance iPSCs. The ETA-VC interlayer functions both as surface modifier for low work function electrode and electron selective layer, reducing contact resistance and improving compatibility and electron transport between the active layer and ITO cathode, while maximizing light absorption within the active layer, leading to remarkable enhancements in J_{SC} and PCE. This approach provides an effective route to fabricate flexible devices and improve their device performance by replacing metal oxide layers with organic surface modifiers in organic optoelectronic devices.

ASSOCIATED CONTENT

Supporting Information

Ultraviolet photoelectron spectroscopy, atomic force microscopy, and contact angle measurement. This material is available free of charge via the Internet at http://pubs.acs.org.

AUTHOR INFORMATION

Corresponding Author

*E-mail: jykim@unist.ac.kr.

Author Contributions

H.C. and H.-B.K contributed equally to this work.

Notes

The authors declare no competing financial interest.

ACKNOWLEDGMENTS

This research was supported by the National Research Foundation of Korea Grant (NRF-2009-0093020, NRF-2013R1A2A2A01015342), the International Cooperation of the Korea Institute of Energy Technology Evaluation and Planning (KETEP) grant funded by the Korea government Ministry of Knowledge Economy (2012T100100740), and the BK21 Plus funded by the Ministry of Education, Korea (10Z20130011057).

REFERENCES

(1) Yu, G.; Gao, J.; Hummelen, J. C.; Wudl, F.; Heeger, A. J. Polymer Photovoltaic Cells: Enhanced Efficiencies via a Network of Internal Donor-Acceptor Heterojunctions. *Science* **1995**, *270*, 1789−1791.

(2) Kim, J. Y.; Lee, K.; Coates, N. E.; Moses, D.; Nguyen, T.-Q.; Dante, M.; Heeger, A. J. Efficient Tandem Polymer Solar Cells Fabricated by All-solution Processing. *Science* **2007**, *317*, 222−225.

(3) Park, S. H. Bulk Heterojunction Solar Cells with Internal Quantum Efficiency Approaching 100%. *Nat. Photonics* **2009**, *3*, 297−302.

(4) He, Z.; Zhong, C.; Su, S.; Xu, M.; Wu, H.; Cao, Y. Enhanced Power-Conversion Efficiency in Polymer Solar Cells Using an Inverted Device Structure. *Nat. Photonics* **2012**, *6*, 591−595.

(5) Chen, H.-C.; Chen, Y.-H.; Liu, C.-C.; Chien, Y.-C.; Chou, S.-W.; Chou, P.-T. Prominent Short-Circuit Currents of Fluorinated

Quinoxaline-Based Copolymer Solar Cells with a Power Conversion Efficiency of 8.0%. *Chem. Mater.* **2012**, *24*, 4766−4772.
(6) Son, H. J.; Lu, L.; Chen, W.; Xu, T.; Zheng, T.; Carsten, B.; Strzalka, J.; Darling, S. B.; Chen, L. X.; Yu, L. Synthesis and Photovoltaic Effect in Dithieno[2,3-d:2′,3′-d′]Benzo[1,2-b:4,5-b′]-dithiophene-Based Conjugated Polymers. *Adv. Mater.* **2013**, *25*, 838−843.
(7) Choi, H.; Ko, S.-J.; Choi, Y.; Joo, P.; Kim, T.; Lee, B. R.; Jung, J.-W.; Choi, H. J.; Cha, M.; Jeong, J.-R.; Hwang, I.-W.; Song, M. H.; Kim, B.-S.; Kim, J. Y. Versatile Surface Plasmon Resonance of Carbon-Dot-Supported Silver Nanoparticles in Polymer Optoelectronic Devices. *Nat. Photonics* **2013**, *7*, 732−738.
(8) Wang, D. H.; Park, K. H.; Seo, J. H.; Seifter, J.; Jeon, J. H.; Kim, J. K.; Park, J. H.; Park, O. O.; Heeger, A. J. Enhanced Power Conversion Efficiency in PCDTBT/$PC_{70}BM$ Bulk Heterojunction Photovoltaic Devices with Embedded Silver Nanoparticle Clusters. *Adv. Energy Mater.* **2011**, *1*, 766−770.
(9) Kim, J. Y.; Kim, S. H.; Lee, H. H.; Lee, K.; Ma, W.; Gong, X.; Heeger, A. J. New Architecture for High-Efficiency Polymer Photovoltaic Cells Using Solution-Based Titanium Oxide as an Optical Spacer. *Adv. Mater.* **2006**, *18*, 572−576.
(10) Peet, J.; Kim, J. Y.; Coates, N. E.; Ma, W. L.; Moses, D.; Heeger, A. J.; Bazan, G. C. Efficiency Enhancement in Low-Band Gap Polymer Solar Cells by Processing with Alkane Dithiols. *Nat. Mater.* **2007**, *6*, 497−500.
(11) Lee, K.; Kim, J. Y.; Park, S. H.; Kim, S. H.; Cho, S.; Heeger, A. J. Air-Stable Polymer Electronic Devices. *Adv. Mater.* **2007**, *19*, 2445−2449.
(12) Chen, L.-M.; Hong, Z.; Li, G.; Yang, Y. Recent Progress in Polymer Solar Cells: Manipulation of Polymer:Fullerene Morphology and the Formation of Efficient Inverted Polymer Solar Cells. *Adv. Mater.* **2009**, *21*, 1434−1449.
(13) Chen, C.-P.; Chen, Y.-D.; Chuang, S.-C. High-Performance and Highly Durable Inverted Organic Photovoltaics Embedding Solution-Processable Vanadium Oxides as an Interfacial Hole-Transporting Layer. *Adv. Mater.* **2011**, *23*, 3859−3863.
(14) Choi, H.; Park, J. S.; Jeong, E.; Kim, G.-H.; Lee, B. R.; Kim, S. O.; Song, M. H.; Woo, H. Y.; Kim, J. Y. Combination of Titanium Oxide and a Conjugated Polyelectrolyte for High-Performance Inverted-Type Organic Optoelectronic Devices. *Adv. Mater.* **2011**, *23*, 2759−2763.
(15) You, J.; Chen, C.-C.; Dou, L.; Murase, S.; Duan, H.-S.; Hawks, S. A.; Xu, T.; Son, H. J.; Yu, L.; Li, G.; Yang, Y. Metal Oxide Nanoparticles as an Electron-Transport Layer in High-Performance and Stable Inverted Polymer Solar Cells. *Adv. Mater.* **2012**, *24*, 5267−5272.
(16) Sun, Y.; Seo, J. H.; Takacs, C. J.; Seifter, J.; Heeger, A. J. Inverted Polymer Solar Cells Integrated with a Low-Temperature-Annealed Sol−Gel-Derived ZnO Film as an Electron Transport Layer. *Adv. Mater.* **2011**, *23*, 1679−1683.
(17) Hsieh, C.-H.; Cheng, Y.-J.; Li, P.-J.; Chen, C.-H.; Dubosc, M.; Liang, R.-M.; Hsu, C.-S. Highly Efficient and Stable Inverted Polymer Solar Cells Integrated with a Cross-Linked Fullerene Material as an Interlayer. *J. Am. Chem. Soc.* **2010**, *132*, 4887−4893.
(18) Jeong, B. S.; Norton, D. P.; Budai, J. D. Conductivity in Transparent Anatase TiO_2 Films Epitaxially Grown by Reactive Sputtering Deposition. *Solid-State Electron.* **2003**, *47*, 2275−2278.
(19) Hofhuis, J.; Schoonman, J.; Goossens, A. Time-of-Flight Studies on TiO_2/$CuInS_2$ Heterojunctions. *J. Appl. Phys.* **2008**, *103*, 014503.
(20) Ma, H.; Yip, H.-L.; Huang, F.; Jen, A. K. Y. Interface Engineering for Organic Electronics. *Adv. Funct. Mater.* **2010**, *20*, 1371−1388.
(21) Yip, H.-L.; Jen, A. K. Y. Recent Advances in Solution-Processed Interfacial Materials for Efficient and Stable Polymer Solar Cells. *Energy Environ. Sci.* **2012**, *5*, 5994−6011.
(22) Yang, H.; Zhu, S.; Pan, N. Studying the Mechanisms of Titanium Dioxide as Ultraviolet-Blocking Additive for Films and Fabrics by an Improved Scheme. *J. Appl. Polym. Sci.* **2004**, *92*, 3201−3210.
(23) Zhou, Y.; Fuentes-Hernandez, C.; Shim, J.; Meyer, J.; Giordano, A. J.; Li, H.; Winget, P.; Papadopoulos, T.; Cheun, H.; Kim, J.; Fenoll, M.; Dindar, A.; Haske, W.; Najafabadi, E.; Khan, T. M.; Sojoudi, H.; Barlow, S.; Graham, S.; Brédas, J.-L.; Marder, S. R.; Kahn, A.; Kippelen, B. A Universal Method to Produce Low−Work Function Electrodes for Organic Electronics. *Science* **2012**, *336*, 327−332.
(24) Na, S.-I.; Kim, T.-S.; Oh, S.-H.; Kim, J.; Kim, S.-S.; Kim, D.-Y. Enhanced Performance of Inverted Polymer Solar Cells with Cathode Interfacial Tuning via Water-Soluble Polyfluorenes. *Appl. Phys. Lett.* **2010**, *97*, 223305.
(25) Beek, W. J. E.; Slooff, L. H.; Wienk, M. M.; Kroon, J. M.; Janssen, R. A. J. Hybrid Solar Cells Using a Zinc Oxide Precursor and a Conjugated Polymer. *Adv. Funct. Mater.* **2005**, *15*, 1703−1707.
(26) Choi, H.; Lee, J.-P.; Ko, S.-J.; Jung, J.-W.; Park, H.; Yoo, S.; Park, O.; Jeong, J.-R.; Park, S.; Kim, J. Y. Multipositional Silica-Coated Silver Nanoparticles for High-Performance Polymer Solar Cells. *Nano Lett.* **2013**, *13*, 2204−2208.
(27) Cowan, S. R.; Roy, A.; Heeger, A. J. Recombination in Polymer-Fullerene Bulk Heterojunction Solar Cells. *Phys. Rev. B* **2010**, *82*, 245207.
(28) Kyaw, A. K. K.; Wang, D. H.; Gupta, V.; Zhang, J.; Chand, S.; Bazan, G. C.; Heeger, A. J. Efficient Solution-Processed Small-Molecule Solar Cells with Inverted Structure. *Adv. Mater.* **2013**, *25*, 2397−2402.
(29) Gupta, V.; Kyaw, A. K. K.; Wang, D. H.; Chand, S.; Bazan, G. C.; Heeger, A. J. Barium: An Efficient Cathode Layer for Bulk-heterojunction Solar Cells. *Sci. Rep.* **2013**, 3.
(30) Wetzelaer, G. A. H.; Kuik, M.; Lenes, M.; Blom, P. W. M. Origin of the Dark-Current Ideality Factor in Polymer:fullerene Bulk Heterojunction Solar Cells. *Appl. Phys. Lett.* **2011**, *99*, 153506.